

IY LYR: A THICK-DISK FIRST-OVERTONE RR LYRAE STAR WITH A POSSIBLE NEUTRON STAR COMPANION

LINJIA LI,¹ SHENGBANG QIAN,^{2,3} ILДАР ASFANDIYAROV,⁴ AZIZBEK MATEKOV,^{1,4,5} LIYING ZHU,^{1,5}
BOONRUCKSAR SOONTHORNTHUM,⁶ EVELINA GAYNULLINA,⁴ ALINA KHALIKOVA,⁴ JIAJIA HE,¹ FANGBIN MENG,^{1,5}
HUITING ZHANG,^{2,3} JIANGJIAO WANG,^{1,5} AND XIANGDONG SHI¹

¹*Yunnan Observatories, Chinese Academy of Sciences, P.O. Box 110, Kunming, 650216, People's Republic of China*

²*Department of Astronomy, School of Physics and Astronomy, Yunnan University, Kunming 650091, People's Republic of China*

³*Key Laboratory of Astroparticle Physics of Yunnan Province, Yunnan University, Kunming 650091, People's Republic of China*

⁴*Ulugh Beg Astronomical Institute, Uzbekistan Academy of Sciences, 33 Astronomicheskaya Street, Tashkent 100052, Uzbekistan*

⁵*University of Chinese Academy of Sciences, No.1 Yanqihu East Rd, Huairou District, Beijing, 101408, People's Republic of China*

⁶*National Astronomical Research Institute of Thailand, 191 Siriphanich Building, Huay Kaew Road, Chiang Mai 50200, Thailand*

Submitted to ApJ

ABSTRACT

IY Lyr, historically misclassified as an eclipsing binary, is now established as a first-overtone RR Lyrae star (RRc star). Using multi-band photometry (ASAS-SN, ZTF, TESS, and our BVRI data), LAMOST spectroscopy, and Gaia astrometry, we investigate its pulsation, binarity, and Galactic population. From O-C analysis, we detect a long-term period decrease and a light-travel time effect with an orbital period of 3.94 years, eccentricity of 0.46, and a mass function of $0.65 M_{\odot}$. The companion is independently confirmed by radial velocity residuals and Gaia proper motions. Combined constraints yield an orbital inclination of 94.8° and a companion mass of $1.37 M_{\odot}$. Chemical abundances ($[\text{Fe}/\text{H}] \simeq -1.0$, $[\alpha/\text{Fe}] \simeq +0.27$, Xiang et al. 2019) and dynamics ($L_z \simeq 1250 \text{ kpc km s}^{-1}$, $Z_{\text{max}} \simeq 1.31 \text{ kpc}$) identify IY Lyr as an old, high- α , thick-disk star. The companion mass lies at the peak of the neutron star mass distribution, and the system's age excludes a main-sequence star; we conclude the companion is most likely a typical neutron star, although a massive white dwarf near the Chandrasekhar limit cannot be ruled out. IY Lyr is among the few RRc binaries with a compact companion verified by multiple methods, and it has important implications for thick-disk binary evolution and neutron star formation.

Keywords: methods: data analysis – stars: fundamental parameters – stars: horizontal-branch – stars: pulsations – stars: variables: RR Lyrae variable

arXiv:2605.05708v1 [astro-ph.SR] 7 May 2026

1. INTRODUCTION

RR Lyrae stars (RRLs) are low-mass pulsating variables located on the horizontal branch, characterized by helium-burning cores and atmospheres that pulsate via the κ -mechanism (Smith 2004; Catelan & Smith 2015). They are primarily classified into ab-type RRLs (RRab stars), which exhibit large-amplitude fundamental-mode pulsations with sawtooth-shaped light curves, and c-type RRLs (RRc stars), which display smaller-amplitude first-overtone pulsations with sinusoidal light curves. Rare d-type RRLs (RRd stars) show dual-mode pulsations (Nemec & Moskalik 2021 and references therein). Studies of their pulsation reveal complex phenomena like the century-old Blazhko effect, a periodic modulation potentially linked to mode coupling, magnetic activity, or resonance (Kolenberg 2011); and the Oosterhoff dichotomy, which offers insights into the Galactic assembly history (refer to Li et al. 2025 and references therein). Their period-luminosity relation makes them essential standard candles for measuring distances, playing a crucial role in both stellar astrophysics and the study of galactic evolution (Smith 2004).

Despite the well-established prevalence of binary systems among stars, confirmed binary RRLs and robust candidates remain exceptionally rare (e.g., Sylla et al. 2024 and references therein). Detecting companions is crucial not only for understanding the binary evolution pathways that lead to old horizontal branch stars but also for improving the precision of RRLs as distance indicators, since binarity can influence their observed properties and period-luminosity calibration. The most widely used detection method exploits the star’s own pulsation as a clock, searching for the light-travel time effect (LTTE) caused by orbital motion through analysis of timing residuals in Observed-minus-Calculated (O-C) diagrams (Sterken 2005). However, this signal can be degenerate with intrinsic period variations typical of these stars (Benkó et al. 2025). Direct detection via eclipses in light curves is highly unlikely due to the stars’ evolutionary history; having previously ascended the red giant branch, they likely possess widely separated companions with long orbital periods¹. To date, only one convincing eclipsing binary system containing an RRL has been identified (OGLE-BLG-RRLYR-02792, Pietrzyński et al. 2012; Smolec et al. 2013). Complementary techniques include radial velocity monitoring, which is observationally intensive due to the need for dense phase coverage, and astrometric analysis using high-precision data from missions like Gaia to detect companion-induced wobble in proper motion (Kervella et al. 2019a,b, 2022). It is anticipated that the release of the next Gaia data set will yield more results in this area². Nonetheless, in the era of large photometric surveys, the O-C method remains the primary discovery tool, with other techniques playing vital roles in confirmation and characterization.

Most RRL binary candidates discovered through the O-C method are RRab stars (Hajdu et al. 2015; Liška et al. 2016; Li et al. 2018; Prudil et al. 2019; Hajdu et al. 2021), while samples of first-overtone RRc stars remain rare. Derezak et al. (2004) reported the discovery of the RRc star BE Dor (MACHO* J050918.712-695015.31), which exhibited rapid period changes and suggested the LTTE in a binary system as a possible explanation. However, follow-up spectroscopic observations found no supporting radial velocity variations, effectively ruling out the binary hypothesis (Derezak et al. 2021). This conclusion was later reinforced by an independent analysis of its complex period variations (Li et al. 2022). A similar case is KIC 2831097, where significant phase variations were initially attributed to binary motion involving an $\geq 8.4 M_{\odot}$ companion (Sódor et al. 2017), but subsequent detailed radial velocity monitoring failed to confirm binarity (Poretti et al. 2025).

On the theoretical modeling front, Bobrick et al. (2024) demonstrated through detailed binary evolution models that metal-rich RRLs may predominantly originate from binary interactions. In such systems, a companion star strips the envelope from a red giant branch primary, causing it to become bluer on the horizontal branch and enter the pulsation instability strip. This evolutionary channel naturally accounts for the existence of young, metal-rich RRLs, which are challenging to explain through single-star evolution, and motivates ongoing searches for such systems (Abdollahi et al. 2025).

Against this backdrop, the star IY Lyr presents an intriguing case. It was historically misclassified as a W Ursae Majoris-type eclipsing binary with a 0.6531646-day period (Hoffmeister et al. 1951), an interpretation followed in several subsequent studies (Malkov et al. 2006; Brát et al. 2008; Coughlin et al. 2014; Qian et al. 2020). However, its true nature as a pulsating RRc variable has been firmly established in modern surveys and catalogs (Kinman & Brown 2014; Sesar et al. 2017; Heinze et al. 2018; Clementini et al. 2019; Chen et al. 2020; Mullen et al. 2022; Clementini et al. 2023). In the Gaia DR3 RRL catalog, IY Lyr is identified as an RRc star with a period of 0.32661639 days and a G-band amplitude of 0.3772 mag (Clementini et al. 2023). Despite this clarification, a dedicated study of IY

¹ <http://spiff.rit.edu/richmond/asras/rrlyr/rrlyr.html>

² <https://www.cosmos.esa.int/web/gaia/dr4>

Lyr, particularly regarding a potential binary companion, has been lacking. Therefore, we monitored it using a 60-cm telescope in Uzbekistan and collected multi-epoch data from several survey projects (see Section 2). Our investigation reveals compelling evidence for a compact companion of approximately 1.4 solar masses. Furthermore, we find IY Lyr to be metal-rich and a member of the thick disk population characteristics that provide important context for its evolutionary status. We present our data analysis in Section 3, followed by discussion and conclusions in Sections 4 and 5.

2. OBSERVATION AND SURVEYS

2.1. Photometric data

Observations of IY Lyr were conducted over 15 nights between September-October 2023 and July-September 2024 using the ZEISS-600 telescope at the Maidanak Astronomical Observatory. This telescope is a 0.6-meter Cassegrain system with a focal ratio of $f/12.5$, making it well suited for high-resolution stellar observations. It is equipped with a scientific-grade FLI IMG ProLine 1024×1024 CCD camera, which provides precise, low-noise imaging. Standard Johnson-Cousin Bessel BVRI filters were used throughout the observing runs. The comparison star was NOMAD-1-1209-0294636 (RA = $18^{\text{h}}:29^{\text{m}}:47.48^{\text{s}}$, Dec = $+30^{\circ}:59':12.57''$), whose BVRI magnitudes (B = 14.2914, V = 13.7291, R = 13.3883, and I = 13.0399) were derived from Gaia G_{BP} , G, and G_{RP} photometry using the transformation relations from Ruelas-Mayorga et al. (2025). The check star was NOMAD-1-1210-0294366 (RA = $18^{\text{h}}:29^{\text{m}}:50.37^{\text{s}}$, Dec = $+31^{\circ}:00':48.00''$), with magnitudes B = 14.4192, V = 13.8812, R = 13.5537, and I = 13.2115. Figure 1 presents the phase-folded light curves in the BVRI bands.

To fully utilize multi-epoch photometric data for the study of IY Lyr, this work combines publicly available data from two major sky surveys: the Zwicky Transient Facility (ZTF) and the All-Sky Automated Survey for Supernovae (ASAS-SN). ZTF employs a wide-field camera at Palomar Observatory to conduct high-cadence photometric surveys, offering high sampling rates and broad sky coverage, which are advantageous for time-domain astronomy (Masci et al. 2019). ASAS-SN, through a global network of small-aperture telescopes, provides long-term, continuous monitoring of bright targets across the entire sky, supplying essential data for analyzing long-term photometric behavior (Shappee et al. 2014). Table 1 summarizes the key information of the photometric data used in this study, including the observation time range, corresponding passband, number of valid data points, and data source, thereby clearly presenting the observational coverage and statistical characteristics of each dataset. Although the space telescope TESS does not provide ready-made light curve products (Ricker et al. 2015), we followed the data reduction approach described in Li et al. (2023) and obtained approximately 32,000 data points. These data will be used for further analysis in Sections 3.1 and 3.2.

In addition, to precisely determine the pulsation phase of IY Lyr, we conducted an additional one-hour observation on the evening of November 25, 2025, using the 85 cm telescope at the Xinglong Observatory of the National Astronomical Observatories, Chinese Academy of Sciences. From these data, a set of times of maximum light was derived for subsequent O-C analysis.

2.2. Spectral information

The Large Sky Area Multi-Object Fiber Spectroscopic Telescope (LAMOST), a major Chinese scientific facility, has conducted medium- and low-resolution spectroscopic observations of IY Lyr (Zhao et al. 2012). Based on these data, several studies have derived stellar physical parameters for this target, including radial velocity, effective temperature, and metallicity (Luo et al. 2018, 2019, 2022; Xiang et al. 2019; Wang et al. 2023, 2024; Zhang et al. 2020, 2022; Ding et al. 2024; Luo et al. 2026). In this work, we primarily adopt the parameters provided by Wang et al. (2024) for further analysis, as their study specifically focuses on RR Lyrae variables and employs a targeted data-processing methodology, making their parameters particularly suitable for our investigation.

2.3. Astrometric data

Astrometric data provide two-dimensional information about the projection of an object's orbit onto the celestial tangent plane. By combining proper motion data from the Hipparcos and Gaia satellites, Kervella et al. (2019a, 2022) developed and applied a method to detect close companions through proper motion anomalies (PMa). This approach was subsequently extended to search for companions of RR Lyrae variables (Kervella et al. 2019b). Inspired by this work, we have developed a new method that, starting from known orbital parameters (e.g., derived from LTTEs or radial velocity measurements), uses differences in proper motion data from different epochs to solve for

the remaining orbital parameters, such as the longitude of the ascending node (Ω) and the orbital inclination (i). A detailed derivation of the method is presented in Section 3.3. Typically, this method requires combining proper motion data from Hipparcos and Gaia. However, IY Lyr is relatively faint and was not recorded in the Hipparcos catalog. We note that the proper motion values reported in Gaia DR2 and Gaia DR3 exhibit significant differences within their respective uncertainties (see Section 3.3 for details). Therefore, in this study, we attempt to use the proper motion differences between the Gaia data releases to constrain and confirm the orbital parameters of IY Lyr.

3. ANALYSIS

In this section, we present a comprehensive analysis to detect and characterize the binary companion of IY Lyr. First, we extract the orbital parameters from the O-C diagram. Next, we independently verify these parameters using radial velocity and astrometric proper motion data. Finally, we determine the system's kinematic properties and its membership within the Galactic population.

3.1. O-C analysis

For pulsating variable stars, the times of light maximum are the most commonly used phase reference for O-C analysis. In this study, 180 times of light maximum for IY Lyr were determined based on multi-epoch photometric data. The following methods were employed to obtain accurate timings according to the characteristics of the different data sources.

1. Data from our own observations using the 60 cm telescope in Uzbekistan and the 85 cm telescope at Xinglong Station: The conventional polynomial fitting method around the light-curve maximum was employed. Specifically, data points near the maximum were selected and fitted with an algebraic polynomial. The time of light maximum was then determined by locating the zero point of the first derivative of the fitted curve (Sterken 2005). This approach is suitable for light curves with relatively high time resolution and dense phase coverage.

2. Survey data (ZTF, ASAS-SN, TESS): Since these data typically cover complete pulsation cycles over extended time baselines, we fitted the entire phase-folded light curves using Fourier series and determined the times of maximum by locating the extrema of the fitted function. The Fourier polynomial is expressed as follow:

$$m(t) = A_0 + \sum_{k=1}^n A_k \sin\left[\frac{2\pi kt}{P_{\text{pul}}} + \phi_k^s\right], \quad (1)$$

where $m(t)$ is the magnitude observed at time t , A_0 is the mean magnitude, A_k and ϕ_k^s are the amplitude and phase of the k -th component, respectively, and P_{pul} is the pulsation period. To account for different noise levels and sampling properties, the order n was chosen as follows: $n = 3$ for ZTF and ASAS-SN data, and $n = 5$ for TESS data due to their higher quality and denser sampling. This approach follows the same strategy as described by Li et al. (2021, 2022).

All determined times of light maximum, along with their associated errors, observational methods, and data sources, are listed in Table 2. Using the corrected linear ephemeris:

$$\text{HJD}_{\text{max}} = 2458291.05844(163) + 0.^{\text{d}}32661702(33) \cdot E, \quad (2)$$

originally comes from Jayasinghe et al. (2018), we calculated the corresponding O-C values and plotted the O-C diagram (upper panel of Figure 2). To describe the linear period change and the possible LTTE, we fitted the data using the following model:

$$O - C = \delta T_0 + \delta P_0 \cdot E + \frac{\beta}{2} E^2 + \tau, \quad (3)$$

where δT_0 and δP_0 are the corrections to the initial epoch and the pulsation period, respectively; β is the linear rate of period change (in day cycle⁻¹); and τ denotes the time delay caused by the LTTE. The expression for τ is:

$$\tau = \left(\frac{a_1 \sin i}{c}\right) [\sqrt{1 - e^2} \sin E^* \cos \omega + \cos E^* \sin \omega], \quad (4)$$

where $a_1 \sin i/c$ represents the projected semi-major axis in days, e is the orbital eccentricity, ω is the longitude of periastron, and E^* denotes the eccentric anomaly (for details, see Li & Qian 2014; Li et al. 2018). In the fitting process, all O-C points were assigned equal weight. The fitting results are presented in Table 3. The parabolic component

corresponds to a period change rate of $\beta = -1.24 \pm 0.14$ days Myr^{-1} , indicating that the pulsation period of IY Lyr is decreasing. After removing the parabolic trend, the O-C residuals exhibit cyclic variations (middle panel of Figure 2), which can be explained by the LTTE. The derived orbital period is $P_{\text{orb}} = 1438.5 \pm 31.4$ days (about 3.94 yr) with an eccentricity of $e = 0.46 \pm 0.15$.

3.2. Orbital component in Radial velocity

To independently verify the binary hypothesis, we analyze radial velocity (RV) variations using spectroscopic observations of IY Lyr from the LAMOST survey. Two epochs are available: a low-resolution spectrum (LRS) obtained on UTC 2015-05-26T17:44:20.26, and a medium-resolution spectrum (MRS) taken on 2020-06-15T16:38:00.00. RV measurements from these spectra—specifically for metal lines and the $\text{H}\alpha$ line—are adopted from Wang et al. (2024). These data contain blended signals, including the systemic velocity of the binary, pulsation-induced velocities, and orbital motion contributions. Our aim is to isolate the orbital component by subtracting the pulsation contribution.

We correct for pulsation-induced RV variations using published RV templates for RR Lyrae stars (Snedden et al. 2017; Braga et al. 2021; Huang et al. 2024). The corrected RVs are listed in Table 4. Several key steps in this process are outlined below:

1. Determination of the Pulsation phase

The observation time is obtained from the DATE-OBS keyword in the LAMOST FITS headers and converted to Heliocentric Julian Date (HJD). To compute the pulsation phase accurately, a linear ephemeris is necessary. Because pulsation modulation may occur, ephemerides can vary between observing epochs. Fortunately, contemporaneous photometry is available for both LAMOST epochs: ASAS-SN observations coincide with the LRS epoch, and TESS observations correspond to the MRS epoch. From these data, we derive the following linear ephemerides:

$$\text{HJD}_{\text{max}} = 2457184.78478 + 0.^{\text{d}}3266093 \cdot E, \quad (5)$$

and

$$\text{HJD}_{\text{max}} = 2459014.84237 + 0.^{\text{d}}3265670 \cdot E. \quad (6)$$

2. Pulsation RV amplitude

The g -band light curve from ZTF shows a pulsation amplitude of 0.48 mag for IY Lyr. Using Equations (5) and (6) from Huang et al. (2024), we convert this to RV amplitudes of 25.1 km s^{-1} for metal lines (Mg) and 35.6 km s^{-1} for $\text{H}\alpha$ line. These amplitudes are then used to scale the template curves prior to subtraction.

3. Phase alignment of templates

The zero point of the Braga et al. (2021) template corresponds to the mean RV epoch, not to light maximum. Therefore, we shift the template phase by $+0.12$ so that the minimum RV of the Mg template aligns with phase 0, as defined above.

4. Offset correction for template mean RV

The mean RV of the Huang et al. (2024) templates is non-zero: -6.325 km s^{-1} for Mg lines and -9.415 km s^{-1} for $\text{H}\alpha$ line. We apply the corresponding offsets to the template values before performing the subtraction.

Figure 3 displays the RV residuals after pulsation subtraction, plotted against time. Green symbols represent RVs derived from Mg lines, while blue symbols correspond to those from $\text{H}\alpha$ lines. The solid black curve illustrates the orbital RV variation predicted from the O-C derived orbital elements; the gray shaded region indicates the 1σ confidence interval obtained through error propagation. A horizontal dotted red line marks the mean systemic velocity, obtained by minimizing the sum of squared residuals between the observed data points and the theoretical orbital curve. The resulting systemic velocities from the different templates are -37.2 , -37.8 , and -36.8 km s^{-1} , with a mean value of -37.3 km s^{-1} , which we adopt as the systemic RV of the IY Lyr binary system.

The agreement between the RV residuals and the predicted orbital curve strongly supports the presence of a companion, corroborating the evidence from O-C analyses. This consistency across independent observational techniques reinforces the binary interpretation of IY Lyr.

3.3. Orbital parameter constraints based on Gaia proper motions

When a star exhibits orbital motion caused by a companion, its proper motion on the celestial sphere consists of two components: the systemic proper motion and the periodic orbital proper motion induced by the binary orbit. Inspired by methods that use proper motion anomalies to detect unseen stellar companions (Kervella et al. 2019a,b, 2022), we

combine results from O-C analysis with proper motion data to further constrain the orbital parameters of the IY Lyr system.

The fitted parameters ($a_1 \sin i$, e , ω , P_{orb} , T) from the O-C analysis provide information on six orbital parameters elements. The quantity $a_1 \sin i$ combines two orbital parameters: the semi-major axis of the pulsating primary star's orbit, a_1 , and the orbital inclination, i . e is the eccentricity, ω the longitude of periastron, P_{orb} the orbital period, and T the time of periastron passage. The seventh parameter, the longitude of the ascending node Ω , remains undetermined. To obtain the complete set of Keplerian orbital elements (a_1 , i , e , ω , P_{orb} , T , and Ω), additional positional or proper motion data on the celestial sphere are required.

A Cartesian coordinate system is defined on the celestial sphere, with the x-axis pointing north along the declination direction and the y-axis pointing east along the right ascension direction. The target's orbital motion, described by the seven parameters mentioned above, yields the components of the orbital position:

$$x_{\text{orb}} = A(\cos E^* - e) + F\sqrt{1 - e^2} \sin E^*, \quad (7)$$

and

$$y_{\text{orb}} = B(\cos E^* - e) + G\sqrt{1 - e^2} \sin E^*, \quad (8)$$

where E^* is the eccentric anomaly as mentioned above, and A, B, F, G are the *Thiele – Innes* constants:

$$A = a_1[\cos \Omega \cos \omega - \sin \Omega \sin \omega \cos i], \quad (9)$$

$$B = a_1[\sin \Omega \cos \omega + \cos \Omega \sin \omega \cos i], \quad (10)$$

$$F = a_1[-\cos \Omega \sin \omega - \sin \Omega \cos \omega \cos i], \quad (11)$$

$$G = a_1[-\sin \Omega \sin \omega + \cos \Omega \cos \omega \cos i]. \quad (12)$$

Differentiating the position with respect to time yields the orbital velocity:

$$\dot{x}_{\text{orb}} = \frac{n}{1 - e \cos E^*} [-A \sin E^* + F\sqrt{1 - e^2} \cos E^*], \quad (13)$$

$$\dot{y}_{\text{orb}} = \frac{n}{1 - e \cos E^*} [-B \sin E^* + G\sqrt{1 - e^2} \cos E^*], \quad (14)$$

with $n = 2\pi/P_{\text{orb}} = K_1\sqrt{1 - e^2}/(a_1 \sin i)$, where K_1 is the semi-amplitude of the radial velocity variation (see Table 3).

The difference in proper motion between two epochs, t_1 and t_2 , arises primarily from changes in orbital motion:

$$\Delta \dot{x}_{\text{mod}} = \dot{x}_{\text{orb}}(t_1) - \dot{x}_{\text{orb}}(t_2), \quad (15)$$

$$\Delta \dot{y}_{\text{mod}} = \dot{y}_{\text{orb}}(t_1) - \dot{y}_{\text{orb}}(t_2). \quad (16)$$

The O-C analysis has provided some orbital parameters, leaving Ω and i as unknowns, with ranges $\Omega \in [0, 360^\circ]$ and $i \in [0, 180^\circ]$. We perform a grid search over this parameter space using a step size of 0.1° . For each (Ω, i) pair, we compute the predicted velocity differences between epochs 2015.5 and 2016.0 and compare them with the observed proper motion anomaly. The optimal parameters are determined by minimizing the following objective function:

$$\chi^2 = \left[\frac{\Delta \dot{x}_{\text{mod}}(\Omega, i) - \Delta \text{pmDE}_{t_1-t_2}}{\Delta \text{pmDE}_{t_1-t_2}} \right]^2 + \left[\frac{\Delta \dot{y}_{\text{mod}}(\Omega, i) - \Delta \text{pmRA}_{t_1-t_2}}{\Delta \text{pmRA}_{t_1-t_2}} \right]^2. \quad (17)$$

in which $\Delta \text{pmDE}_{t_1-t_2} = 0.7305 \text{ km s}^{-1}$ and $\Delta \text{pmRA}_{t_1-t_2} = -0.4229 \text{ km s}^{-1}$ represent the proper motion differences between Gaia DR2 and DR3 (Gaia Collaboration et al. 2018, 2023). The conversion from proper motion to radial velocity uses the parallax $Plx = 0.2466 \text{ mas}$ (Gaia Collaboration et al. 2023) and the relation $Vr = 4.74 \text{ pm}/Plx$.

The objective function yields an optimal solution: $\Omega = 218.3 \pm 14.8^\circ$, $i = 94.8 \pm 1.1^\circ$ (errors estimated via Monte Carlo simulation). The grid search also reveals a secondary local solution: $\Omega = 81.7 \pm 14.9^\circ$, $i = 85.2 \pm 1.3^\circ$. This secondary solution is confidently excluded based on LAMOST radial velocity data. Figure 4 shows the celestial projection of the orbits for the target star (black curve) and its companion (red curve). The green and blue arrows indicate the orbital velocities (in mas yr^{-1}) at the Gaia DR2 and Gaia DR3 epochs, respectively. The black arrow represents the systemic proper motion of the binary system.

It is important to note that proper motion data trace the motion of the system’s photocenter. If the companion’s luminosity is negligible (e.g., a compact object or exoplanet), the photocenter’s semi-major axis equals that of the primary star, $a_{\text{photo}} = a_1$, which is the assumption in the calculation above. For a companion with non-negligible luminosity, $a_{\text{photo}} = q'a_1$ with $q' < 1$, where

$$q' = 1 - \frac{m_1 + m_2}{m_2} \frac{L_2}{L_1 + L_2}. \quad (18)$$

In the equation, m_1 and m_2 are the masses of the primary and companion star, respectively, while L_1 and L_2 denote their luminosities. This relationship can be derived from the formulation provided by Van De Kamp (1967) in terms of the magnitude difference between the two components, and is equivalent to that presented in Feng et al. (2024). For IY Lyr, the O-C analysis suggests a lower limit for the companion’s mass of approximately $1.4 M_{\odot}$. If the companion is a dark compact object (e.g., a massive white dwarf near the Chandrasekhar limit or a neutron star), then $q' = 1$. If it is a main-sequence star (spectral type F5, luminosity $\sim 5-6 L_{\odot}$), then $q' \approx 0.85$. We systematically explored the parameter space for q' ranging from 1.0 to 0.8, corresponding to the companion’s fractional light contribution from 0% to approximately 10%. For each value of q' , we repeated the grid search to obtain the corresponding (Ω, i) . The results, presented in Figure 5, show that as q' decreases from 1.0 to 0.85, Ω increases from 218.3° to 221.5° , and i increases from 94.8° to 95.7° . Although these shifts are statistically significant, their amplitudes are modest, indicating that the primary star dominates the system’s light and that the orbital parameters are not highly sensitive to the companion’s luminosity. However, based on the analysis of the system’s nature presented in Section 4, a main-sequence companion can be excluded. Therefore, we adopt the solution for $q' = 1$, which yields $i = 94.8^{\circ}$. This inclination is used in all subsequent calculations.

3.4. Kinematic Parameters and Galactic Population Classification

To determine the kinematic properties and population membership of the IY Lyr system within the Galaxy, we combined data from various sources for a comprehensive kinematic analysis. The core observational parameters are listed in Table 5. Positional information was obtained from the CDS website³, while radial velocity and proper motion were derived from Sections 3.2 and 3.3, respectively. The distance was calculated using Gaia DR3 parallax data. We employed the Galpy package⁴ to compute the orbital parameters of the IY Lyr system within the Galactic potential (Bovy 2015). The calculations utilized the Milky Way potential model from McMillan (2017), which includes multiple mass components such as a dark matter halo, stellar disk, and Galactic bulge, providing an accurate description of the Galactic gravitational potential distribution. The adopted solar position and kinematic parameters for the calculations were: Solar Galactocentric distance $R_0 = 8.20$ kpc, circular velocity at the Solar position $v_0 = 232.8$ km s⁻¹, and Solar motion relative to the Local Standard of Rest $(U_{\odot}, V_{\odot}, W_{\odot}) = (11.1, 12.24, 7.25)$ km s⁻¹ (Schönrich et al. 2010; Zinn et al. 2020). By performing a numerical integration of the orbit over 5 Gyr with a time step of 0.5 Myr, we obtained the system’s complete orbital parameters. The resulting dynamical parameters are listed in Table 5, including angular momentum components, total energy, spatial positions and velocity components, as well as characteristic parameters derived from the orbital integration.

The results presented in Table 5 show that the system’s Z-component angular momentum ($L_z = 1249.96$ kpc km s⁻¹) exhibits clear prograde motion. Its value lies between the high angular momentum typical of thin disk stars and the near-zero values characteristic of halo stars, falling within the typical range for thick disk stars (800 - 1800 kpc km s⁻¹). Orbital integration indicates that its maximum height above the Galactic plane ($z_{\text{max}} = 1.31$ kpc) is significantly greater than that of the thin disk (typically < 0.5 kpc) but lower than that of typical halo stars (> 3 kpc). Its low orbital eccentricity ($= 0.279$) further supports its classification as a disk star. In velocity space, both the system’s tangential velocity ($V_{\phi} = 177.09$ km s⁻¹) and peculiar velocity with respect to the Local Standard of Rest ($V_{\text{pec}} = 82.63$ km s⁻¹) fall within the typical dispersion range for thick disk stars, well below the threshold commonly used to distinguish halo stars (Bensby et al. 2014; Zinn et al. 2020). Crucially, its chemical signature of metal-poor but α -enhanced composition ($[\text{Fe}/\text{H}] \simeq -1.0$, $[\alpha/\text{Fe}] \simeq +0.27$; Wang et al. 2024; Xiang et al. 2019), aligns consistently with the kinematic characteristics of moderate prograde angular momentum and high velocity dispersion observed here, forming a synergistic combination distinctive of the thick disk population.

³ <http://simbad.cds.unistra.fr/simbad/>

⁴ <https://github.com/jobovy/galpy>

Based on the age-metallicity relation established by Xiang & Rix (2022) from precise subgiant measurements, the IY Lyr system is a member of the old, high- α thick disc population that formed at ~ 13 Gyr. Its high $[\alpha/\text{Fe}]$ and low $[\text{Fe}/\text{H}]$ place it at the metal-poor end of the early disc’s extremely tight age-metallicity sequence.⁵ This indicates formation during the initial chemical enrichment phase when only core-collapse supernovae had contributed. The high angular momentum, $L_z = 1249.96$ kpc km s⁻¹ demonstrates that this star has remained on a disc-like orbit, escaping significant kinematic heating during the Gaia-Sausage-Enceladus merger approximately 11 Gyr ago. Therefore, it represents a surviving relic of the primordial Milky Way disc that was not ”splashed” into the halo (Belokurov et al. 2020).

4. DISCUSSIONS

4.1. Mass and period evolution of the pulsating primary star

To determine the mass of the RRc star IY Lyr, we utilize BaSTI α -enhanced canonical evolutionary models, considering two metallicity cases: $Z = 0.002$ ($[\text{Fe}/\text{H}] = -1.31$) and $Z = 0.004$ ($[\text{Fe}/\text{H}] = -1.01$) (Pietrinferni et al. 2006). Based on the horizontal-branch evolutionary parameters, we compute the first-overtone pulsation period using the equation provided by Marconi et al. (2015). The LAMOST LRS spectrum was obtained at the pulsation phase of approximately 0.4, corresponding to a temperature that represents the mean temperature over the entire pulsation cycle. Multiple studies have estimated this temperature to lie in the range of 6800 - 7200 K (Luo et al. 2018, 2019, 2022; Xiang et al. 2019; Wang et al. 2023, 2024; Zhang et al. 2020, 2022; Ding et al. 2024; Luo et al. 2026), which we adopt as the mean (intrinsic) temperature of IY Lyr. In the period-temperature diagram (see Figure 6), the evolutionary tracks for masses of 0.61 and 0.62 M_\odot at $Z = 0.002$, and for 0.59 and 0.60 M_\odot at $Z = 0.004$, intersect the observed pulsation period (0.3266 days) within the temperature range of IY Lyr (see Figure 6). Averaging these values yields a pulsating primary star mass of approximately 0.61 M_\odot , which we adopt as the basis for further discussion.

Based on the BaSTI evolutionary tracks corresponding to the mass and metallicity of IY Lyr, the predicted secular period change rate for a horizontal-branch RRc star is typically on the order of ~ 0.01 day Myr⁻¹. This value is approximately two orders of magnitude smaller in absolute terms than the observed parabolic term, $\beta = -1.24 \pm 0.14$ day Myr⁻¹, derived from the O-C analysis. Therefore, the parabolic trend cannot be attributed to a genuine evolutionary period decrease. Instead, it more plausibly represents a long-segment, non-periodic irregular variation commonly observed in some RRc stars (Percy & Tan 2013), which can be empirically modeled by a quadratic term. Importantly, the periodic component of the O-C residuals, which we interpret as the LTTE caused by a binary companion, is independently confirmed by radial velocity and astrometric proper motion analyses (Sections 3.2 and 3.3). Hence, while the parabolic term reflects irregular pulsation behavior, the cyclic signal provides robust evidence for binarity.

4.2. Nature of the companion

Based on the orbital inclination and the mass of the pulsating primary, the mass function indicates a companion mass of $1.37 \pm 0.19 M_\odot$. The system’s age exceeds 10 Gyr, ruling out the possibility that the companion is an F-type main-sequence star. Binary evolution models for RR Lyrae systems also exclude the scenario of an accreting main-sequence companion, as such systems would evolve into RR Lyrae variables earlier (< 9 Gyr) due to the larger mass of the progenitor of the pulsating star (Bobrick et al. 2024). Therefore, the pulsating primary likely formed through single-star evolution, while the more massive companion is expected to be a compact object resulting from more advanced evolutionary stages.

The mass of 1.37 M_\odot lies at the intersection between the upper mass limit for white dwarfs (Chandrasekhar limit $\sim 1.44 M_\odot$) and the peak of the typical neutron star mass distribution ($\sim 1.35 M_\odot$), allowing the companion to be interpreted either as a massive O-Ne-Mg white dwarf near the mass limit or as a typical neutron star. If the companion is a white dwarf, its mass would exceed the natural upper limit predicted by single-star evolution ($\sim 1.1 M_\odot$) (Weidemann 2000), necessitating mass growth via accretion through binary interactions. However, the IY Lyr system has a relatively long orbital period, corresponding to a separation of several astronomical units. The current primary is a 0.61 M_\odot RRc star, and its main-sequence progenitor had a mass of only about 1.0 M_\odot , which could not provide sufficient stellar wind or stable Roche-lobe overflow to enable effective accretion and achieve a mass increase

⁵ The term ”metal-poor” here is used in the context of typical Galactic stellar population studies; in the field of RR Lyrae stars, this metallicity is not considered within the metal-poor regime.

of approximately 0.2 - 0.3 M_{\odot} . Even during the primary’s red giant phase, wind accretion would be subject to considerable uncertainties in efficiency and total accreted mass. Moreover, from a statistical perspective, forming a white dwarf with a mass so close to the Chandrasekhar limit requires finely tuned initial conditions and evolutionary parameters, making such objects rare in observed samples.

In contrast, interpreting the companion as a neutron star does not require additional assumptions about accretion-driven growth. A mass of 1.37 M_{\odot} lies well within the core range of the neutron star mass distribution and can be naturally produced via core-collapse supernova from a progenitor with an initial mass of approximately 8 - 12 M_{\odot} (You et al. 2025). Although supernova explosions typically impart significant kick velocities to newly formed neutron stars (Lyne & Lorimer 1994; Lai et al. 2001; Hobbs et al. 2005; Kalogera et al. 2008), which could disrupt wide binaries, systems with low kick velocities or more compact initial orbits may survive to the present day. Considering measurement uncertainties, the likelihood that the companion’s mass falls below the typical lower limit for neutron stars ($\sim 1.1 M_{\odot}$) is small, while values near or exceeding 1.44 M_{\odot} remain fully consistent with the neutron star interpretation. In summary, in the absence of direct evidence such as pulsed signals or accretion-powered X-rays, identifying the companion of IY Lyr as a typical neutron star represents the most parsimonious interpretation that is globally consistent with the observational data. Future improvements in mass precision through more accurate photometric and radial-velocity measurements, or the detection of radio pulsations or X-ray emission from the companion, will be crucial for confirming its true nature.

4.3. Comparison with the Results of Hajdu et al. (2021)

Hajdu et al. (2021) presented a statistical analysis of RR Lyrae binary candidates based on OGLE data toward the Galactic bulge, finding that the mass function distribution exhibits a trimodal shape, corresponding to companion masses of approximately 0.6, 0.2, and 0.067 M_{\odot} , respectively. Among their sample, the star OGLE-BLG-RRLYR-20376 (hereafter OGLE-20376) shows a high degree of similarity in orbital parameters to IY Lyr, as presented in this work ($P_{\text{orb}} = 1641$ days, $a_1 \sin i = 2.330$ AU, $e = 0.628$, $f(m) = 0.66507 M_{\odot}$). Both stars have very similar orbital periods, projected semi-major axes, and mass functions. Their mass functions are significantly higher than the highest peak of the trimodal distribution reported in Hajdu et al. (2021), implying a minimum companion mass of about 1.4 M_{\odot} and suggesting the possibility of a massive white dwarf or a neutron star companion.

Despite their similar orbital parameters, IY Lyr and OGLE-20376 differ in their Galactic population membership. Although OGLE-20376 is located in the direction of the bulge, our dynamical analysis using Gaia data and the radial velocity from Luongo et al. (2024) shows that its orbital characteristics are consistent with the Galactic halo population. Its orbit is highly eccentric (~ 0.82), typical of halo stars with radial, deeply penetrating orbits; the maximum height above the Galactic plane reaches $Z_{\text{max}} = 4.174$ kpc, far exceeding the thick-disk scale height and consistent with halo membership. The angular momentum about the Galactic Z -axis is very low ($L_z = 314.42$ kpc km s $^{-1}$), indicating negligible net rotation around the Galactic center. Additionally, its peculiar velocity relative to the Local Standard of Rest is extremely high ($V_{\text{pec}} = 319$ km s $^{-1}$), well above the typical dispersion of disk stars (see Table 5). Furthermore, literature reports extremely low photometric metallicities for this star, down to $[\text{Fe}/\text{H}] = -2.52$ (Luongo et al. 2024) and $[\text{Fe}/\text{H}] = -3.212$ (Dékány & Grebel 2022), supporting its classification as a very old halo star. This indicates that the two stars belong to the thick disk and the halo, respectively, representing different star formation and evolutionary histories.⁶

Overall, the bulge sample of Hajdu et al. (2021) is characterized by a predominance of low-mass companions (white dwarfs, red dwarfs, and brown dwarfs), with orbital periods primarily concentrated between 3000 and 4000 days and an eccentricity peak near 0.25 to 0.3. In contrast, IY Lyr (a thick disk RRc star) and OGLE-20376 (a halo RRab star) exhibit similar orbital parameters but have mass functions significantly higher than the typical values observed in the bulge sample, despite belonging to different Galactic substructures. The rarity of systems with such high mass functions in the bulge sample may reflect their intrinsic scarcity within the bulge. Variations among Galactic substructures in star formation rate, initial mass function, metallicity evolution, and binary interaction history likely contribute to the diversity in formation efficiency and the distribution of orbital parameters in compact companion binary systems (Bobrick et al. 2024).

⁶ It should be noted that Huson et al. (2025) derived a metallicity of $[\text{Fe}/\text{H}] = -0.83$ for OGLE-20376 using the deep learning model Gaia Net on Gaia DR3 low-resolution spectra. If this value is accurate, combined with its low angular momentum, $L_z = 314$ kpc km s $^{-1}$, the star could be a ‘splashed’ thick disk star resulting from the merger with the Gaia-Sausage-Enceladus satellite galaxy (Belokurov et al. 2020; Xiang & Rix 2022).

It is important to emphasize that comparisons based on only one or a few high-mass function systems are insufficient to draw universal conclusions. The orbital similarity between IY Lyr and OGLE-20376 may be coincidental, or it may indicate a specific formation channel (e.g., survival of a primordial massive binary after a supernova explosion) that operates efficiently in different environments. A systematic expansion of RR Lyrae binary candidate samples in the thick disk, halo, and bulge, combined with high-precision radial velocity and metallicity measurements, will be essential to distinguish between these possibilities and to gain a deeper understanding of the formation and evolution of RR Lyrae binaries across different Galactic substructures.

4.4. Extending the PMA Method via the q' Parameter and Prospects with Gaia DR4

In Section 3.3, we introduced the parameter q' to quantify the contribution of the companion's luminosity to the system's photocenter. This extension significantly broadens the applicability of the classical PMA method. Previously, the method was limited to cases where the companion's luminosity was negligible (e.g., compact objects or exoplanets). With the inclusion of q' , the analysis can now be extended to systems in which the companion's light is significant, such as those hosting main-sequence companions. This provides a more general physical basis for constraining the orbital inclination i and the longitude of the ascending node Ω using astrometric data.

It should be noted, however, that IY Lyr was not observed by the Hipparcos satellite. Consequently, we cannot utilize the classical PMA approach, which leverages the ~ 25 yr time baseline between Hipparcos and Gaia to amplify the orbital motion signal. As an alternative, we employed the proper motion difference between Gaia DR2 and Gaia DR3; however, the time span between these two epochs is only about 0.5 years. Given the system's orbital period of 3.94 year, this relatively short baseline may weaken the orbital signal in the proper motion difference, thereby reducing the precision of the derived i and Ω .

Looking ahead, the forthcoming Gaia DR4 will provide time-series astrometric data rather than epoch-averaged proper motions. This advancement will enable us to directly model the orbital motion of the IY Lyr system through a joint fit, effectively overcoming the current limitation imposed by a short baseline (e.g., the result of [Gaia Collaboration et al. 2024](#)). With Gaia DR4, we will significantly improve the accuracy of the orbital parameters and independently verify the conclusions drawn from the proper motion difference analysis presented here. This development offers a promising pathway toward ultimately determining the nature of the companion and its formation channel.

5. SUMMARY

In this study, we conducted a comprehensive analysis of the pulsation characteristics, binary orbital motion, and Galactic population membership of the RRc star IY Lyr. Our investigation utilized multi-band time-series photometry (ASAS-SN, ZTF, TESS, and our own BVRI observations), LAMOST spectroscopy, and Gaia astrometry. By cross-validating the O-C method, radial velocity residuals, and proper motion anomaly analysis, we reveal for the first time that this star hosts a compact companion. Furthermore, we precisely constrain its orbital parameters, physical properties, and stellar population affiliation. The main conclusions are as follows:

1. Confirmation of IY Lyr as an RRc star and detection of binary orbital motion

The O-C diagram reveals a long-term period decrease at a rate of $\beta = -1.24 \pm 0.14$ day Myr $^{-1}$, superimposed by a LTTE with an orbital period of $P_{\text{orb}} = 1438.5 \pm 31.4$ days (≈ 3.94 years), eccentricity $e = 0.46 \pm 0.15$, and mass function $f(m) = 0.65 \pm 0.14 M_{\odot}$.

2. Independent verification of the companion and determination of its nature

The LAMOST radial velocities, after subtracting the pulsational contribution, agree well with the orbital velocity curve predicted by the O-C solution. Using the proper motion difference between Gaia DR2 and DR3, together with the O-C parameters, we derive an orbital inclination $i = 94.8^{\circ} \pm 1.1^{\circ}$, leading to a companion mass $M_2 = 1.37 \pm 0.19 M_{\odot}$. The system's age exceeds 10 Gyr, ruling out a main-sequence companion. This mass lies at the peak of the neutron star mass distribution and does not require accretion growth, making a typical neutron star the most plausible interpretation; however, a massive white dwarf near the Chandrasekhar limit cannot be completely excluded.

3. IY Lyr belongs to the old, thick-disk population of the Milky Way.

Dynamical integration yields an angular momentum $L_z = 1249.96$ kpc km s $^{-1}$, a maximum height above the Galactic plane $z_{\text{max}} = 1.23$ kpc, and an orbital eccentricity $e = 0.279$. Combined with its metallicity ($[\text{Fe}/\text{H}] \simeq -1.0$) and α enhancement ($[\alpha/\text{Fe}] \simeq +0.27$), IY Lyr is identified as an old (~ 13 Gyr), high- α thick disk star, providing observational support for binary evolution channels that produce RR Lyrae stars.

In summary, IY Lyr is one of the very few RRc stars with a compact companion ($\simeq 1.4 M_{\odot}$) that has been independently confirmed through O-C, radial velocity, and astrometric methods. It represents the first clear case of

such a system in the thick disk. This work also extends the classical proper motion anomaly method by introducing the photocentric weight factor q' , making it applicable to systems where the companion contributes a non-negligible amount of light. Future Gaia DR4 time-series astrometry will enable further refinement of the orbital parameters and ultimately help confirm the true nature of the companion. Our finding carries important implications for thick-disc binary evolution and the formation channels of neutron stars in binary systems.

This work is supported by the International Cooperation Projects of the National Key R&D Program (No. 2022YFE0127300), the International Partnership Program of Chinese Academy of Sciences (No. 020GJHZ2023030GC), the Yunnan Fundamental Research Projects (grant Nos. 202503AP140013, 202501AS070055, 202401AS070046), the China Manned Space Program with grant no. CMS-CSST-2025-A16, the CAS "Light of West China" Program and "Yunnan Revitalization Talent Support Program" in Yunnan Province. We acknowledge the support of the staff of the ZEISS-600 telescope at the Maidanak Astronomical Observatory and the Xinglong 2.16m/85cm telescope. This work was partially supported by National Astronomical Observatories, Chinese Academy of Sciences.

Based on observations obtained with the Samuel Oschin Telescope 48-inch and the 60-inch Telescope at the Palomar Observatory as part of the Zwicky Transient Facility project. ZTF is supported by the National Science Foundation under Grants No. AST-1440341 and AST-2034437 and a collaboration including current partners Caltech, IPAC, the Oskar Klein Center at Stockholm University, the University of Maryland, University of California, Berkeley, the University of Wisconsin at Milwaukee, University of Warwick, Ruhr University, Cornell University, Northwestern University and Drexel University. Operations are conducted by COO, IPAC, and UW. This paper includes data collected with the TESS mission, obtained from the MAST data archive at the Space Telescope Science Institute (STScI). Funding for the TESS mission is provided by the NASA Explorer Program. STScI is operated by the Association of Universities for Research in Astronomy, Inc., under NASA contract NAS 5-26555. The specific observations analyzed can be accessed via [<https://doi.org/10.17909/3y7c-wa45>]. This work has made use of data from the European Space Agency (ESA) mission *Gaia* (<https://www.cosmos.esa.int/gaia>), processed by the *Gaia* Data Processing and Analysis Consortium (DPAC, <https://www.cosmos.esa.int/web/gaia/dpac/consortium>). Funding for the DPAC has been provided by national institutions, in particular the institutions participating in the *Gaia* Multilateral Agreement. This work also utilizes photometric data from ASAS-SN database (Shappee et al. 2014; Jayasinghe et al. 2018, 2019a,b, 2020, 2021; Christy et al. 2023).

REFERENCES

- Abdollahi, H., Molnár, L., & Varga, V. 2025, *A&A*, 695, L14
- Belokurov, V., Sanders, J. L., Fattahi, A., et al. 2020, *MNRAS*, 494, 3880
- Benkő, J. M., Bódi, A., Plachy, E., & Molnár, L. 2025, *A&A*, 697, A154
- Bensby, T., Feltzing, S., & Oey, M. S. 2014, *A&A*, 562, A71
- Bobrick, A., Iorio, G., Belokurov, V., et al. 2024, *MNRAS*, 527, 12196
- Bovy, J. 2015, *ApJS*, 216, 29
- Braga, V. F., Crestani, J., Fabrizio, M., et al. 2021, *ApJ*, 919, 85
- Brát, L., Šmelcer, L., Kuèáková, H., et al. 2008, *Open European Journal on Variable Stars*, 0094, 1
- Catelan, M., & Smith, H. A. 2015, *Pulsating Stars*
- Chen, X., Wang, S., Deng, L., et al. 2020, *ApJS*, 249, 18
- Christy, C. T., Jayasinghe, T., Stanek, K. Z., et al. 2023, *MNRAS*, 519, 5271
- Clementini, G., Ripepi, V., Molinaro, R., et al. 2019, *A&A*, 622, A60
- Clementini, G., Ripepi, V., Garofalo, A., et al. 2023, *A&A*, 674, A18
- Coughlin, J. L., Thompson, S. E., Bryson, S. T., et al. 2014, *AJ*, 147, 119
- Dékány, I., & Grebel, E. K. 2022, *ApJS*, 261, 33
- Derekas, A., Kiss, L. L., Udalski, A., Bedding, T. R., & Szatmáry, K. 2004, *MNRAS*, 354, 821
- Derekas, A., Thompson, I. B., Bokon, A., et al. 2021, in *Posters from the TESS Science Conference II (TSC2)*, 53
- Ding, M.-Y., Shi, J.-R., Yan, H.-l., et al. 2024, *ApJS*, 271, 58
- Feng, F., Rui, Y., Xuan, Y., & Jones, H. 2024, *ApJS*, 271, 50
- Gaia Collaboration, Brown, A. G. A., Vallenari, A., et al. 2018, *A&A*, 616, A1
- Gaia Collaboration, Vallenari, A., Brown, A. G. A., et al. 2023, *A&A*, 674, A1
- Gaia Collaboration, Panuzzo, P., Mazeh, T., et al. 2024, *A&A*, 686, L2

- Hajdu, G., Catelan, M., Jurcsik, J., et al. 2015, *MNRAS*, 449, L113
- Hajdu, G., Pietrzyński, G., Jurcsik, J., et al. 2021, *ApJ*, 915, 50
- Heinze, A. N., Tonry, J. L., Denneau, L., et al. 2018, *AJ*, 156, 241
- Hobbs, G., Lorimer, D. R., Lyne, A. G., & Kramer, M. 2005, *MNRAS*, 360, 974
- Hoffmeister, C., Rohlf, E., & Ahnert, P. 1951, *Veroeffentlichungen der Sternwarte Sonneberg*, 1, 407
- Huang, Y., Fang, M., Liu, G., et al. 2024, *Research in Astronomy and Astrophysics*, 24, 075009
- Huson, D., Cowan, I., Sizemore, L., Kounkel, M., & Hutchinson, B. 2025, *ApJ*, 984, 58
- Jayasinghe, T., Kochanek, C. S., Stanek, K. Z., et al. 2018, *MNRAS*, 477, 3145
- Jayasinghe, T., Stanek, K. Z., Kochanek, C. S., et al. 2019a, *MNRAS*, 485, 961
- 2019b, *MNRAS*, 486, 1907
- 2020, *MNRAS*, 491, 13
- Jayasinghe, T., Kochanek, C. S., Stanek, K. Z., et al. 2021, *MNRAS*, 503, 200
- Kalogera, V., Valsecchi, F., & Willems, B. 2008, in *American Institute of Physics Conference Series*, Vol. 983, 40 Years of Pulsars: Millisecond Pulsars, Magnetars and More, ed. C. Bassa, Z. Wang, A. Cumming, & V. M. Kaspi (AIP), 433–441
- Kervella, P., Arenou, F., Mignard, F., & Thévenin, F. 2019a, *A&A*, 623, A72
- Kervella, P., Arenou, F., & Thévenin, F. 2022, *A&A*, 657, A7
- Kervella, P., Gallenne, A., Remage Evans, N., et al. 2019b, *A&A*, 623, A116
- Kinman, T. D., & Brown, W. R. 2014, *AJ*, 148, 121
- Kolenberg, K. 2011, in *RR Lyrae Stars, Metal-Poor Stars, and the Galaxy*, ed. A. McWilliam, Vol. 5, 100
- Lai, D., Chernoff, D. F., & Cordes, J. M. 2001, *ApJ*, 549, 1111
- Li, L.-J., & Qian, S.-B. 2014, *MNRAS*, 444, 600
- Li, L.-J., Qian, S.-B., Shi, X.-D., & Zhu, L.-Y. 2023, *AJ*, 166, 83
- Li, L.-J., Qian, S.-B., & Zhu, L.-Y. 2018, *ApJ*, 863, 151
- 2022, *MNRAS*, 510, 6050
- Li, L.-J., Qian, S.-B., Zhu, L.-Y., He, J.-J., & Fang, X.-H. 2021, *AJ*, 161, 193
- Li, L.-J., Qian, S.-B., Zhu, L.-Y., Shi, X.-D., & Liao, W.-P. 2025, *MNRAS*, 542, 1791
- Liška, J., Skarka, M., Zejda, M., Mikulášek, Z., & de Villiers, S. N. 2016, *MNRAS*, 459, 4360
- Luo, A.-L., Zhao, Y.-H., Zhao, G., & et al. 2018, *VizieR Online Data Catalog: LAMOST DR4 catalogs (Luo+, 2018)*, *VizieR On-line Data Catalog: V/153*. Originally published in: 2018RAA..in.prep..L, ,
- 2019, *VizieR Online Data Catalog: LAMOST DR5 catalogs (Luo+, 2019)*, *VizieR On-line Data Catalog: V/164*. Originally published in: 2019RAA..in.prep..L, ,
- 2022, *VizieR Online Data Catalog: LAMOST DR7 catalogs (Luo+, 2019)*, *VizieR On-line Data Catalog: V/156*. Originally published in: 2019RAA..in.prep..L, ,
- 2026, *VizieR Online Data Catalog: LAMOST DR11 catalogs (Luo+, 2026)*, *VizieR On-line Data Catalog: V/162*. Originally published in: 2026RAA..in.prep..L, ,
- Luongo, E., Ripepi, V., Marconi, M., et al. 2024, *A&A*, 690, L17
- Lyne, A. G., & Lorimer, D. R. 1994, *Nature*, 369, 127
- Malkov, O. Y., Oblak, E., Snegireva, E. A., & Torra, J. 2006, *A&A*, 446, 785
- Marconi, M., Coppola, G., Bono, G., et al. 2015, *ApJ*, 808, 50
- Masci, F. J., Laher, R. R., Rusholme, B., et al. 2019, *PASP*, 131, 018003
- McMillan, P. J. 2017, *MNRAS*, 465, 76
- Mullen, J. P., Marengo, M., Martínez-Vázquez, C. E., et al. 2022, *ApJ*, 931, 131
- Nemec, J. M., & Moskalik, P. 2021, *MNRAS*, 507, 781
- Percy, J. R., & Tan, P. J. 2013, *Journal of the American Association of Variable Star Observers (JAAVSO)*, 41, 75
- Pietrinferni, A., Cassisi, S., Salaris, M., & Castelli, F. 2006, *ApJ*, 642, 797
- Pietrzyński, G., Thompson, I. B., Gieren, W., et al. 2012, *Nature*, 484, 75
- Poretti, E., Le Borgne, J. F., Correa, M., et al. 2025, *A&A*, 703, A286
- Prudil, Z., Skarka, M., Liška, J., Grebel, E. K., & Lee, C.-U. 2019, *MNRAS*, 487, L1
- Qian, S.-B., Zhu, L.-Y., Liu, L., et al. 2020, *Research in Astronomy and Astrophysics*, 20, 163
- Ricker, G. R., Winn, J. N., Vanderspek, R., et al. 2015, *Journal of Astronomical Telescopes, Instruments, and Systems*, 1, 014003
- Ruelas-Mayorga, A., Macías-Estrada, E., Sánchez, L. J., et al. 2025, *RAS Techniques and Instruments*, 4, rzaf037
- Schönrich, R., Binney, J., & Dehnen, W. 2010, *MNRAS*, 403, 1829
- Sesar, B., Hernitschek, N., Mitrović, S., et al. 2017, *AJ*, 153, 204
- Shappee, B. J., Prieto, J. L., Grupe, D., et al. 2014, *ApJ*, 788, 48
- Smith, H. A. 2004, *RR Lyrae Stars*

- Smolec, R., Pietrzyński, G., Graczyk, D., et al. 2013, MNRAS, 428, 3034
- Snedden, C., Preston, G. W., Chadid, M., & Adamów, M. 2017, ApJ, 848, 68
- Sódor, Á., Skarka, M., Liška, J., & Bognár, Z. 2017, MNRAS, 465, L1
- Sterken, C. 2005, in *Astronomical Society of the Pacific Conference Series*, Vol. 335, *The Light-Time Effect in Astrophysics: Causes and cures of the O-C diagram*, ed. C. Sterken, 3
- Sylla, S., Kolenberg, K., Klotz, A., et al. 2024, A&A, 691, A108
- Van De Kamp, P. 1967, *Principles of astrometry*
- Wang, J., Shi, J., Fu, J., Zong, W., & Li, C. 2024, ApJS, 272, 31
- Wang, R., Luo, A.-L., Zhang, S., et al. 2023, ApJS, 266, 40
- Weidemann, V. 2000, A&A, 363, 647
- Xiang, M., & Rix, H.-W. 2022, Nature, 603, 599
- Xiang, M., Ting, Y.-S., Rix, H.-W., et al. 2019, ApJS, 245, 34
- You, Z.-Q., Zhu, X., Liu, X., et al. 2025, Nature Astronomy, 9, 552
- Zhang, B., Liu, C., & Deng, L.-C. 2020, ApJS, 246, 9
- Zhang, B., Jing, Y.-J., Yang, F., et al. 2022, ApJS, 258, 26
- Zhao, G., Zhao, Y.-H., Chu, Y.-Q., Jing, Y.-P., & Deng, L.-C. 2012, *Research in Astronomy and Astrophysics*, 12, 723
- Zinn, R., Chen, X., Layden, A. C., & Casetti-Dinescu, D. I. 2020, MNRAS, 492, 2161

Table 1. Summary of photometric data used in this work for IY Lyr.

Source	Time Range (HJD-2400000)	Band/ Filter	Data Points (N)	Typical Error (mag)
ASAS-SN	56595 - 58414	<i>V</i>	310	0.0241
ZTF	58204 - 60610	<i>zg</i>	1205	0.0111
	58197 - 60610	<i>zr</i>	1432	0.0101
	58229 - 60576	<i>zi</i>	176	0.0112
TESS	56303 - 57799	TESS	32113	-
Maidanak60cm	60189 - 60568	<i>B</i>	670	0.0057
	60189 - 60568	<i>V</i>	674	0.0049
	60189 - 60568	<i>R_c</i>	670	0.0053
	60189 - 60568	<i>I_c</i>	671	0.0064
Xinglong85cm	61004 - 61004	<i>V</i>	25	0.0050
	61004 - 61004	<i>R</i>	25	0.0050

Notes. ASAS-SN: All-Sky Automated Survey for Supernovae (Shappee et al. 2014). ZTF: Zwicky Transient Facility (Masci et al. 2019).

TESS: Transiting Exoplanet Survey Satellite (Ricker et al. 2015). Its overall operating band range is approximately 600 to 1000 nanometers. Maidanak60: 60 cm telescope at Maidanak Astronomical Observatory. XL85cm: 85 cm telescope at XingLong Observatory.

Table 2. The 180 new available times of light maximum for UY Cam obtained from the sky surveys, literature and our observations.

HJD.	Error	Ref.	HJD.	Error	Ref.	HJD.	Error	Ref.	HJD.	Error	Ref.
2400000+	(days)		2400000+	(days)		2400000+	(days)		2400000+	(days)	
56788.9325	0.0062	ASASSN	59057.9497	0.0037	ZTF(zg)	60139.3681	0.0100	ZTF(zr)	60332.7391	0.0025	TESS
56846.4140	0.0058	ASASSN	59060.2461	0.0032	ZTF(zr)	60155.7163	0.0024	ZTF(zg)	60334.0371	0.0023	TESS
56906.1868	0.0079	ASASSN	59115.7698	0.0097	ZTF(zg)	60189.3574	0.0012	60cm(R)	60335.0212	0.0066	TESS
57115.1968	0.0065	ASASSN	59135.0401	0.0034	ZTF(zr)	60189.3577	0.0013	60cm(B)	60335.9992	0.0016	TESS
57184.7848	0.0086	ASASSN	59299.3331	0.0065	ZTF(zr)	60189.3591	0.0016	60cm(V)	60336.9762	0.0023	TESS
57253.3847	0.0047	ASASSN	59353.5499	0.0076	ZTF(zi)	60189.3592	0.0022	60cm(I)	60337.9642	0.0023	TESS
57469.5681	0.0085	ASASSN	59388.8266	0.0065	ZTF(zr)	60192.2749	0.0011	60cm(B)	60338.9385	0.0023	TESS
57552.8761	0.0179	ASASSN	59392.0902	0.0011	TESS	60192.2777	0.0011	60cm(V)	60425.8078	0.0037	ZTF(zr)
57608.4084	0.0063	ASASSN	59394.3700	0.0046	ZTF(zg)	60192.2843	0.0019	60cm(I)	60425.8103	0.0031	ZTF(zg)
57847.1722	0.0037	ASASSN	59395.0304	0.0018	TESS	60192.2854	0.0019	60cm(R)	60480.3611	0.0026	TESS
57911.5206	0.0040	ASASSN	59398.3016	0.0016	TESS	60195.2282	0.0010	60cm(V)	60481.3417	0.0021	TESS
57972.2778	0.0069	ASASSN	59404.5045	0.0012	TESS	60195.2290	0.0011	60cm(B)	60482.3217	0.0017	TESS
58221.5147	0.0025	ZTF(zg)	59408.0972	0.0013	TESS	60195.2294	0.0010	60cm(R)	60483.3002	0.0030	TESS
58233.5818	0.0105	ASASSN	59411.0388	0.0027	TESS	60195.2409	0.0018	60cm(I)	60486.5873	0.0084	TESS
58242.4179	0.0019	ZTF(zr)	59413.9792	0.0015	TESS	60196.2130	0.0012	60cm(V)	60488.5452	0.0034	TESS
58262.9897	0.0034	ZTF(zg)	59415.2792	0.0117	ZTF(zi)	60196.2139	0.0011	60cm(B)	60489.5141	0.0033	TESS
58270.8151	0.0066	ZTF(zi)	59416.9206	0.0013	TESS	60196.2143	0.0010	60cm(R)	60490.4966	0.0045	TESS
58288.4477	0.0047	ASASSN	59472.1042	0.0066	ZTF(zi)	60196.2180	0.0022	60cm(I)	60491.4685	0.0060	TESS
58304.7949	0.0031	ZTF(zg)	59478.6353	0.0054	ZTF(zr)	60197.1923	0.0019	60cm(R)	60492.4508	0.0042	TESS
58305.4462	0.0028	ZTF(zr)	59481.5972	0.0080	ZTF(zg)	60197.1929	0.0020	60cm(B)	60493.7588	0.0030	TESS
58314.9056	0.0073	ZTF(zi)	59699.4427	0.0173	ZTF(zr)	60197.1933	0.0015	60cm(V)	60494.7346	0.0024	TESS
58338.7575	0.0050	ZTF(zr)	59707.2788	0.0045	ZTF(zg)	60197.1976	0.0026	60cm(I)	60495.7119	0.0043	ZTF(zg)
58345.9390	0.0055	ZTF(zg)	59729.8277	0.0078	ZTF(zi)	60209.2673	0.0012	60cm(R)	60495.7137	0.0021	TESS
58358.9968	0.0067	ZTF(zi)	59748.4468	0.0067	TESS	60209.2729	0.0030	60cm(I)	60496.6960	0.0035	TESS
58360.3025	0.0018	ASASSN	59751.3972	0.0086	TESS	60209.2749	0.0011	60cm(V)	60497.6791	0.0020	TESS
58394.6124	0.0025	ZTF(zr)	59754.3223	0.0016	TESS	60209.2752	0.0016	60cm(B)	60498.6531	0.0020	TESS
58401.7930	0.0028	ZTF(zg)	59761.5104	0.0059	TESS	60217.1122	0.0085	ZTF(zr)	60499.9618	0.0026	TESS
58588.6053	0.0038	ZTF(zg)	59764.4473	0.0096	TESS	60225.6125	0.0049	ZTF(zg)	60500.9435	0.0019	TESS
58598.0771	0.0038	ZTF(zr)	59767.3896	0.0018	TESS	60313.4641	0.0046	TESS	60501.9251	0.0023	TESS
58647.3958	0.0015	ZTF(zg)	59771.3073	0.0013	TESS	60314.4416	0.0032	TESS	60502.9067	0.0024	TESS
58661.7684	0.0024	ZTF(zr)	59774.2440	0.0016	TESS	60315.4184	0.0042	TESS	60502.9085	0.0045	ZTF(zr)
58664.0522	0.0054	ZTF(zi)	59777.5190	0.0066	TESS	60316.4008	0.0026	TESS	60503.8910	0.0058	TESS
58685.6041	0.0031	ZTF(zg)	59780.4503	0.0013	TESS	60317.3841	0.0028	TESS	60504.8620	0.0040	TESS
58721.2129	0.0036	ZTF(zg)	59781.4272	0.0059	ZTF(zg)	60319.3444	0.0033	TESS	60514.3362	0.0011	60cm(V)
58739.8317	0.0051	ZTF(zr)	59784.0435	0.0013	TESS	60320.6488	0.0018	TESS	60514.3368	0.0023	60cm(R)
58767.5974	0.0042	ZTF(zg)	59787.6399	0.0014	TESS	60321.6304	0.0021	TESS	60514.3379	0.0011	60cm(B)
58957.3588	0.0041	ZTF(zg)	59788.9330	0.0083	ZTF(zr)	60322.6122	0.0020	TESS	60514.3443	0.0021	60cm(I)
58984.7841	0.0043	ZTF(zr)	59790.2427	0.0056	ZTF(zi)	60323.5893	0.0022	TESS	60556.7925	0.0103	ZTF(zg)
59011.9059	0.0017	TESS	59790.5827	0.0054	TESS	60324.5687	0.0017	TESS	60568.2298	0.0015	60cm(B)
59014.8424	0.0022	TESS	59846.7522	0.0123	ZTF(zi)	60325.5446	0.0024	TESS	60568.2307	0.0015	60cm(V)
59017.7836	0.0016	TESS	59860.7974	0.0040	ZTF(zr)	60327.8393	0.0056	TESS	60568.2356	0.0017	60cm(R)
59021.3802	0.0026	TESS	59860.8033	0.0024	ZTF(zg)	60328.8122	0.0027	TESS	60568.2420	0.0028	60cm(I)
59024.6441	0.0017	TESS	60067.5226	0.0061	ZTF(zr)	60329.7895	0.0024	TESS	60573.7784	0.0058	ZTF(zr)
59027.5848	0.0045	TESS	60076.3574	0.0035	ZTF(zi)	60330.7674	0.0024	TESS	61004.9324	0.0014	85cm(V)
59030.8468	0.0012	TESS	60084.5075	0.0033	ZTF(zg)	60331.7571	0.0022	TESS	61004.9336	0.0014	85cm(R)

Notes. 60cm: 60 cm telescope at Maidanak Astronomical Observatory. 85cm: 85 cm telescope at XingLong Observatory.

Table 3. The pulsating and orbital elements of AX UMa. P_{orb} is the orbital period, T is the time of passage through the periastron, $f(M)$ is the mass function of the companion, K_1 is the velocity semi-amplitude in km s^{-1} , and χ^2 is residual sum of Squares.

Parameter	LTTE fitting
$T_0[\text{cor}]$	2458291.05922(119)
$P_{\text{pul}}[\text{cor}](\text{days})$	0.32662127(36)
β (d cycle $^{-1}$)	$-1.11(.12) \times 10^{-9}$
β (d Myr $^{-1}$)	-1.24(.14)
$a_1 \sin i/c$ (d)	0.01247(89)
$a_1 \sin i$ (au)	2.16(.15)
e	0.46(.15)
ω ($^\circ$)	135.1(18.3)
P_{orb} (d)	1438.5(31.4)
P_{orb} (yr)	3.938(86)
T	2458384.7(72.4)
$f(M)$ (M_\odot)	0.65(.14)
K_1 (km s^{-1})	18.35(2.08)
χ^2	1642.754

Table 4. Radial velocities of IY Lyr corrected for pulsational variations using templates from Sneden et al. (2017); Braga et al. (2021); Huang et al. (2024).

Obs Time		Wang2024		Sneden2017		Braga2021		Huang2024	
HJD	Pulsation	Vr_metal	Vr_α	Vr_m_cor	Vr_α_cor	Vr_m_cor	Vr_α_cor	Vr_m_cor	Vr_α_cor
2400000+	Phase	km s^{-1}	km s^{-1}	km s^{-1}	km s^{-1}	km s^{-1}	km s^{-1}	km s^{-1}	km s^{-1}
LRS									
57169.2419	0.41	-38.5(2.9)	-38.5(1.8)	-42.2	-43.4	-42.5	-46.0	-41.5	-42.3
MRS									
59016.1797	0.10	-49.4(0.7)	-54.0(1.1)	-37.6	-33.2	-37.3	-34.3	-35.8	-36.4
59016.1964	0.15	-45.8(0.6)	-50.4(0.7)	-36.4	-32.9	-36.6	-33.4	-34.4	-34.2
59016.2123	0.20	-43.5(0.5)	-46.4(1.3)	-36.9	-33.0	-37.1	-33.2	-35.2	-32.8

Table 5. The Galactic positions and the kinematics of the IY Lyr system and OGLE-BLG-RRLYR-20376 (OGLE-20376) system.

Parameter	IY Lyr	OGLE-20376	Source/Description
Observation Parameters			
Right Ascension (α , J2000) [°]	277.41987	263.23184	CDS
Declination (δ , J2000) [°]	31.00016	-22.76635	CDS
Parallax (ϖ) [mas]	0.2466	0.2495	GaiaDR3
Distance (d) [kpc]	4.055	4.008	($1/\varpi$)
System Proper Motion in RA ($\mu\alpha*\cos\delta$) [mas yr ⁻¹]	-10.823	-2.023	This work/GaiaDR3
System Proper Motion in Dec ($\mu\delta$) [mas yr ⁻¹]	-1.958	-5.578	This work/GaiaDR3
System Radial Velocity (V_r) [km s ⁻¹]	-37.3	228.4	This work/Luongo et al. (2024)
Current Position & Velocity			
Galactocentric Radius (R) [kpc]	7.06	4.237	Projected distance from Galactic Center
Height above Galactic Plane (Z) [kpc]	1.26	0.408	Current vertical height
Radial Velocity (V_R) [km s ⁻¹]	58.28	-235.64	Galactocentric radial velocity
Tangential Velocity (V_T or V_ϕ) [km s ⁻¹]	177.09	74.21	Azimuthal velocity
Vertical Velocity (V_Z) [km s ⁻¹]	17.12	144.89	Velocity perpendicular to the Galactic plane
Peculiar Velocity (V_{pec}) [km s ⁻¹]	82.63	319.00	Velocity relative to LSR
angular Momentum & energy			
L_Z [kpc km s ⁻¹]	1249.96	314.42	Angular momentum about galactic Z-axis
L_\perp [kpc km s ⁻¹]	228.34	710.77	Angular momentum perpendicular to Z-axis
Total Energy (E_{tot}) [(km s ⁻¹) ²]	-171795.27	-176243.29	Sum of kinetic and potential energy
Orbital Characteristics			
Maximum height above Plane (Z_{max}) [kpc]	1.314	4.174	Maximum vertical excursion from orbit integration
Pericentre Distance (R_{peri}) [kpc]	4.365	0.852	Closest approach to Galactic Center
Apocentre Distance (R_{apo}) [kpc]	7.737	8.612	Farthest point from Galactic Center
Orbital Eccentricity	0.279	0.820	$(R_{apo}-R_{peri})/(R_{apo}+R_{peri})$
Orbital inclination [°]	$\simeq 10.4$	$\simeq 66.1$	Estimated from $\arctan(L_\perp/L_Z)$

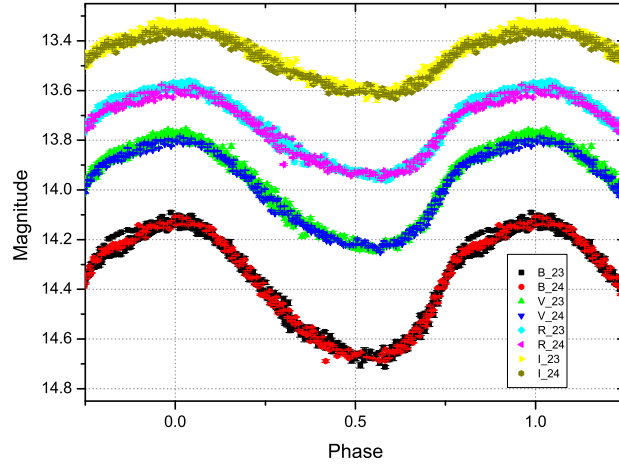


Figure 1. The phased BVRI light curves obtained from the ZEISS-600 telescope located at the Maidanak Astronomical Observatory. The phases are calculated by the linear ephemeris $\text{HJD}_{\text{MAX}} = 2460209.2725775 + 0^{\text{d}}.32661702 \cdot E$.

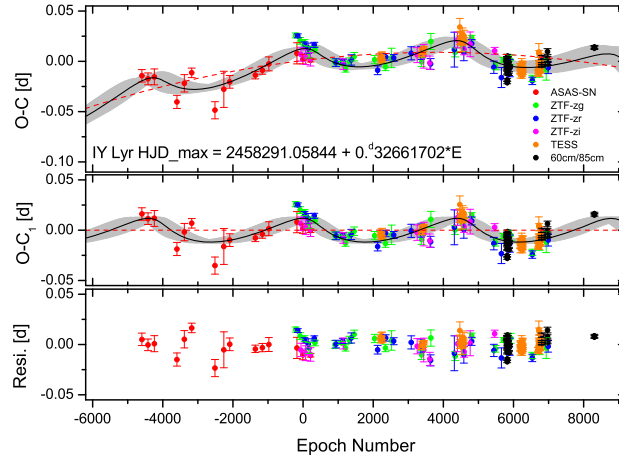


Figure 2. Upper panel: The O-C diagram for IY Lyr. The black solid line refer to a combination of downward parabolic and periodic variations. The red dashed line represent the parabolic variation. The light gray shaded area represents the range within one standard deviation of the best-fit model. Middle panel: The O-C residuals from the quadratic term ($O-C_1$) to IY Lyr. The black solid line refer to the periodic variation. Bottom panel: The O-C residuals from the both quadratic term and the periodic variation (Resi.) to IY Lyr.

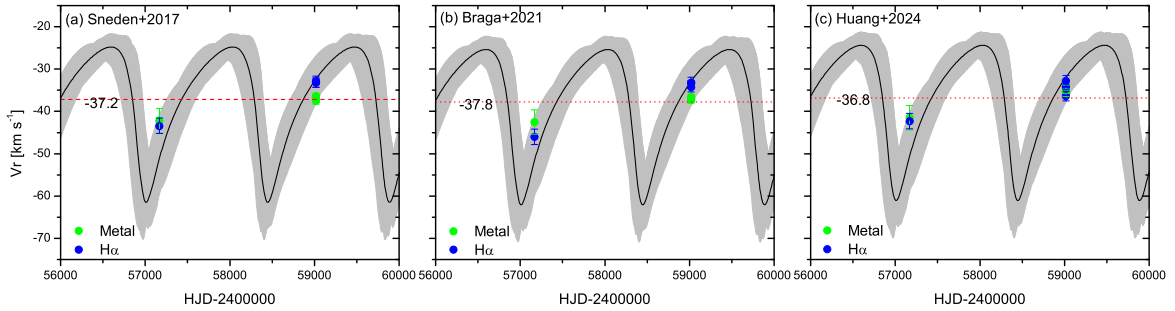


Figure 3. Pulsation-corrected radial velocities of IY Lyr as a function of time. The corrections are applied using three different template sets: (a) Sneden et al. (2017), (b) Braga et al. (2021), and (c) Huang et al. (2024). The solid curves show the orbital radial velocity variations predicted from the O-C solution. The light gray shaded area represents the range within one standard deviation of the best-fit model. The good agreement between the corrected velocities and the predicted curves independently confirms the binary interpretation.

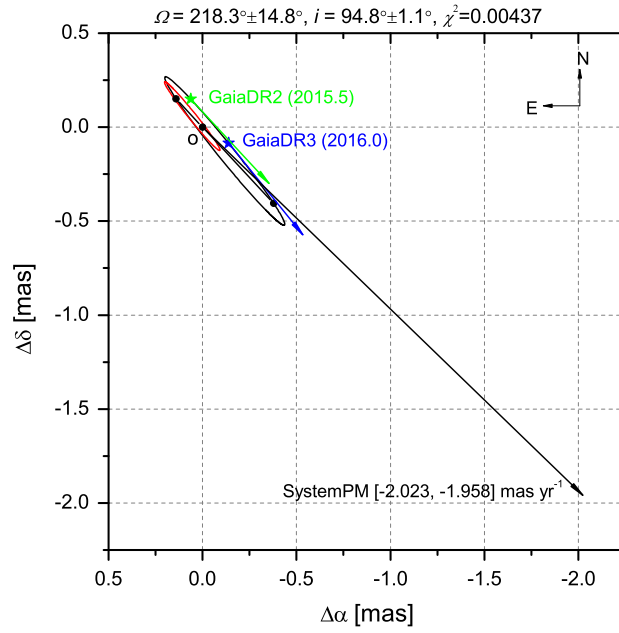


Figure 4. Projected orbits of the IY Lyr binary system on the celestial plane for $\Omega = 218.3^\circ \pm 14.8^\circ$, and $i = 94.8^\circ \pm 1.1^\circ$. The black curve shows the orbit of the pulsating primary star, and the red curve shows the orbit of the unseen compact companion. The green and blue arrows indicate the orbital velocities (in mas yr^{-1}) at the Gaia DR2 and Gaia DR3 epochs, respectively. The black arrow represents the systemic proper motion of the binary system.

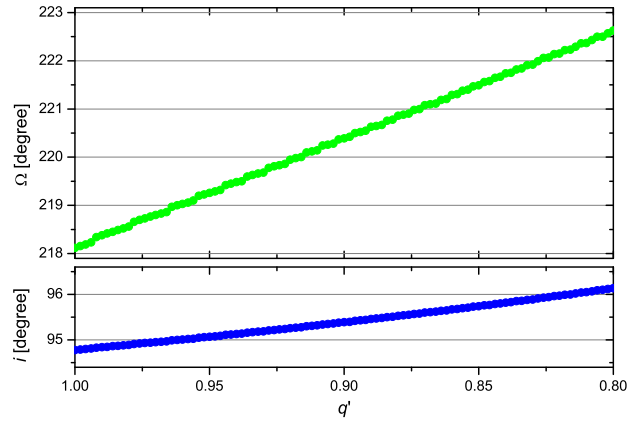


Figure 5. Variation of the orbital parameters Ω (longitude of the ascending node) and i (inclination) as a function of the photocentric weight q' . Only modest changes are seen, confirming the robustness of the orbital solution against the unknown luminosity of the companion.

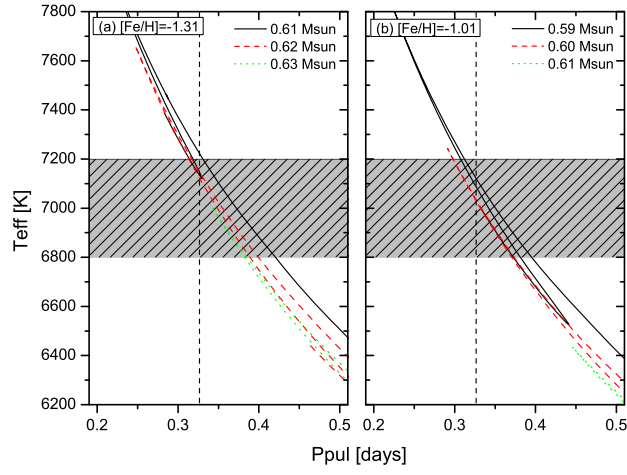


Figure 6. Period - temperature diagrams for IY Lyr. Evolutionary tracks from BaSTI models for $[\text{Fe}/\text{H}] = -1.31$ and -1.01 are shown. The observed period (0.3266 days) and temperature range (6800 - 7200 K) intersect the tracks at masses of 0.61 - 0.62 M_{\odot} ($[\text{Fe}/\text{H}] = -1.31$) and 0.59 - 0.60 M_{\odot} ($[\text{Fe}/\text{H}] = -1.01$), yielding a primary mass of $\sim 0.61 M_{\odot}$.